Journal of Aerosol Science 77 (2014) 127–144

Contents lists available at ScienceDirect

Journal of Aerosol Science

journal homepage: www.elsevier.com/locate/jaerosci

Critical cluster size cannot in practice be determined by slope analysis in atmospherically relevant applications

Oona Kupiainen-Määttä [a,*], Tinja Olenius [a], Hannele Korhonen [b,c], Jussi Malila [d], Miikka Dal Maso [e], Kari Lehtinen [b,d], Hanna Vehkamäki [a]

[a] University of Helsinki, Department of Physics, P.O. Box 64, FI-00014, Finland
[b] Finnish Meteorological Institute, P.O. Box 1627, FI-70211 Kuopio, Finland
[c] Currently at Finnish Meteorological Institute, FI-00101 Helsinki, Finland
[d] University of Eastern Finland, Department of Applied Physics, P.O. Box 1627, FI-70211 Kuopio, Finland
[e] Tampere University of Technology, Department of Physics, P.O. Box 527, FI-33101 Tampere, Finland

ARTICLE INFO

Article history:
Received 24 February 2014
Received in revised form
27 June 2014
Accepted 8 July 2014
Available online 16 July 2014

Keywords:
Atmospheric aerosols
New-particle formation
Nucleation theorem
Modeling
Data analysis

ABSTRACT

The first nucleation theorem is the most widely used method to assess atmospheric new-particle formation mechanisms from particle formation rate measurements. The theorem states that the slope $(\partial \log J)/(\partial \log C)$ of the nucleation rate J versus the concentration C of a nucleating compound gives the number of molecules of that species in the critical cluster. In principle, the derivation of the theorem is solid, but it contains very restrictive assumptions, the validity of which is questionable in realistic situations. It applies only for systems where clusters grow by addition of single molecules, and there are no external losses. In addition, application of the theorem to experimental data requires that the nucleation rate can be determined from particle concentration observations. This work presents simulation results on particle formation rates in atmospherically relevant conditions. We show that the slope of the nucleation rate in realistic conditions differs from that in an ideal situation. The slope analysis can easily lead to erroneous conclusions on the critical cluster size, and should therefore not be used to interpret experimental data.

1. Introduction

Formation of aerosol particles from precursor vapors is an important and widely studied topic in the field of atmospheric sciences. Numerous experimental and theoretical studies have focused on assessing the formation mechanism of aerosols in varying environments (Kulmala et al., 2004; Young et al., 2008; Zhang et al., 2012). The phenomenon begins with vapor-phase molecules colliding with each other to form small molecular clusters and continues with the clusters growing by further collisions, at the same time also being able to lose molecules by evaporation. While sulfuric acid has been recognized as the key compound of the process in many environments (Sihto et al., 2006; Weber et al., 1996), identities and roles of other compounds still remain uncertain.

The gas-to-liquid phase transition related to the particle formation process is in general assumed to proceed via nucleation, where the cluster formation free energy surface exhibits an energy barrier that the growing cluster must

* Corresponding author. Tel.: +358 50 3182220.
E-mail address: oona.kupiainen@helsinki.fi (O. Kupiainen-Määttä).

http://dx.doi.org/10.1016/j.jaerosci.2014.07.005
0021-8502/

overcome in order to become a stable particle. Another option is barrierless condensation, where already the smallest clusters are stable and particle formation is kinetically limited. In case of nucleation, the location of the energy barrier is called the critical cluster size. Clusters that are smaller than the critical size are more likely to evaporate into smaller sizes than to grow further, and clusters that are larger than the critical size are more likely to grow than to decay. A central question concerning the nucleation mechanism is the size and composition of the critical cluster. As cluster energies cannot be measured directly, the critical cluster cannot simply be identified from the energy profile of the nucleating system. A seemingly easy-to-use, and thus very widely employed, method to deduce indirectly the composition of the critical cluster from experimental observations is the first nucleation theorem. According to its most generally used form, the number of molecules of any compound i in the critical cluster, n_i^*, is approximately equal to the slope of the logarithm of the nucleation rate J as a function of the logarithm of the gas-phase concentration C_i of the compound i:

$$\frac{\partial \log J}{\partial \log C_i} \approx n_i^*, \tag{1}$$

where other parameters such as temperature and concentrations of other vapors are assumed to be constant. As sulfuric acid has been identified as the main driving compound of atmospheric new-particle formation, several studies have focused on determining the number of sulfuric acid molecules in the critical cluster (Zhang, 2010; Zollner et al., 2012). In experimental studies, this is normally done by measuring particle concentrations at different sulfuric acid concentrations, determining the particle formation rate at each point, and applying a linear fit to the data presented on a log-log scale. Consequently, the observed formation rate is often reported as a power law $J \propto [H_2SO_4]^x$ (Kuang et al., 2008; Riipinen et al., 2007; Sihto et al., 2006). However, different experiments have given values for the exponent x ranging from 1.3 to 12.9 (Ball et al., 1999; Benson et al., 2008; Brus et al., 2010; Sipilä et al., 2010; Zollner et al., 2012), and the measured formation rates at similar H_2SO_4 concentrations have varied by several orders of magnitude. The formation rate is normally given at the assumed critical cluster size corresponding to a mobility diameter of 1–2 nm. On the other hand, the detection limit of particle counters is often significantly higher than the assumed critical size, and thus the formation rate at the size of interest must be calculated from the particle concentrations at the observed size by assuming a certain growth rate, and accounting for possible losses between these sizes (Kerminen & Kulmala, 2002; Korhonen et al., 2014; Lehtinen et al., 2007).

The nucleation theorem has also been widely used in fundamental nucleation studies not directly related to atmospheric aerosols. Critical cluster sizes determined using the nucleation theorem for measured nucleation rates of various molecular liquids have been compared with theoretical predictions using the classical liquid droplet model. For n-butanol, Viisanen & Strey (1994) found reasonably close agreement between the two approaches, although the slope values were slightly higher than the classical results. On the other hand, Brus et al. (2005) found later large discrepancies between critical cluster sizes of n-butanol determined using different measurement set-ups. For the ethanol–hexanol mixture, Strey & Viisanen (1993) found qualitative agreement between the critical cluster composition determined from measurements and theory, while especially the critical cluster size of pure hexanol deviated by several tens of percent between the slope approach and the liquid drop model. Also in the n- and i-octane mixture, Vehkamäki & Ford (2001) found notable differences between slope values and classical theory. Slope values that are considerably lower than classical predictions have been reported for n-propanol (Brus et al., 2006) and slopes slightly lower than predicted have also been observed for n-pentanol (Hrubý et al., 1996). Also for water, classical predictions may be slightly or even significantly higher than experimental results, especially for larger critical sizes or higher temperatures (Fransen et al., 2013; Manka et al., 2010 and references therein), but there are also some discrepancies between different experimental data sets (see Kim et al., 2004; Manka et al., 2010 and references therein).

Some recent studies (Ehrhart & Curtius 2013; Kupiainen et al., 2013; Malila et al., 2011, 2013) have pointed out that external losses affect the nucleation rate and thus the applicability of the nucleation theorem. In addition to requiring that there are no losses, the derivation of the nucleation theorem also involves several other assumptions. In this work, we present an overview of the derivation, and examine how breaking each of the assumptions affects the results obtained by applying the theorem. While our examples are related to atmospheric new-particle formation, the problems raised in this study are quite general and may affect the applicability of the nucleation theorem also in other systems.

We use a cluster population dynamics model to simulate the formation rate of sulfuric acid–base clusters at a mobility diameter of approximately 1.5 nm, a size at which experimental particle formation rates are often reported. We present the simulated formation rate and its slope with respect to sulfuric acid and base concentrations as a function of acid concentration, and show that the slope may be altered by various factors.

To study the uncertainties related to calculating the formation rate of sub-2-nm particles from the concentrations of larger particles, we also apply a separate aerosol microphysics model to simulate particle growth from 1.5 nm to larger sizes. In this case, the formation rate at 1.5 nm is assumed to follow a power-law dependence $J \propto [H_2SO_4]^x$. The nucleation rate is then back-calculated from the concentrations of 3–6 nm particles following the procedure used in the analysis of experimental data. We show that the exponent x obtained from the slope of the calculated nucleation rate differs from the actual value used as input in the growth simulation, leading to erroneous conclusions about the critical cluster size.

2. The first nucleation theorem

Relation (1), usually referred to as the first nucleation theorem, was first developed on the basis of the classical capillary drop model by Nielsen (1964), who applied it to crystallization from a melt. Kashchiev (1982) gave the result a more general

theoretical footing, still in the capillary drop framework, and coined the term "nucleation theorem". Later, other derivations have been constructed which rely less on the formation energy. The most simplified proof for the single-component case is that by McGraw & Wu (2003) (see also Ford, 1997) which we present below briefly. Let us denote the steady-state concentration of a k-molecule cluster by c_k and its "constrained equilibrium" concentration (that is, the concentration it would have in an equilibrium distribution where the monomer had the supersaturated concentration c_1) by $c_{k,0}$. Taking into account only monomer additions and evaporations, the net flux between each pair of consecutive cluster sizes is

$$I_k = \beta_{1,k} c_1 c_k - \gamma_{1,k} c_{k+1}, \tag{2}$$

where $\beta_{1,k}$ is the collision coefficient between a monomer and a k-molecule cluster and $\gamma_{1,k} = \beta_{1,k} c_1 c_{k,0}/c_{k+1,0}$ is the evaporation rate of a monomer from the $k+1$-molecule cluster, related by detailed balance to the collision rate and the constrained equilibrium distribution. In the absence of external losses, the rate of change of each cluster concentration can be expressed in terms of collision and evaporation fluxes as $\mathrm{d}c_k/\mathrm{d}t = I_{k-1} - I_k$. As in steady-state the concentrations are time-independent, $\mathrm{d}c_k/\mathrm{d}t = 0$, the flux I_k through the system of clusters is equal for all sizes k. It is also equal to the flux at the critical size, or the nucleation rate, denoted as J. Rearranging the terms, summing the birth-death equations for each cluster size and assuming that $c_k/c_{k,0} \to 0$ as $k \to \infty$, the nucleation rate can be written as

$$J = \left(\sum_{k=1}^{\infty} \frac{1}{\beta_{1,k} c_1 c_{k,0}} \right)^{-1}. \tag{3}$$

The constrained equilibrium cluster concentrations follow the law of mass action,

$$K_k = \frac{c_{k,0}}{c_1 c_{k-1,0}}, \tag{4}$$

where K_k is the equilibrium constant, which only depends on temperature and can also be expressed in terms of cluster free energies. Equation (4) results in the power law $c_{k,0} \propto c_1^k$ for the equilibrium cluster concentrations. From this, it can directly be seen that

$$\frac{\mathrm{d}(c_1 c_{k,0})}{\mathrm{d}c_1} = (k+1)\frac{c_1 c_{k,0}}{c_1}, \tag{5}$$

and the derivative of the nucleation rate (3), keeping the temperature, T, and thereby the rates coefficiens, constant, can be calculated to give

$$\left(\frac{\partial \log J}{\partial \log c_1} \right)_T = \frac{\sum_{n=1}^{\infty} \frac{n}{\beta_{1,n} c_{n,0}}}{\sum_{k=1}^{\infty} \frac{1}{\beta_{1,k} c_{k,0}}} + 1 \equiv \overline{n} + 1. \tag{6}$$

If the distribution $1/(\beta_{1,n} c_{n,0})$ has one high maximum at n^* that dominates the sum $\sum_{n=1}^{\infty} n/(\beta_{1,n} c_{n,0})$, the value $\overline{n}$ is approximately equal to n^*. Finally, taking into account the relation between constrained equilibrium concentrations and cluster formation energies, the expression inside the summation becomes

$$\frac{1}{\beta_{1,n} c_{n,0}} \propto \frac{1}{\beta_{1,n}} \exp\left(\frac{\Delta G_n}{k_B T} \right),$$

where ΔG_n is the Gibbs free energy of formation of the n-molecule cluster and k_B is the Boltzmann constant. If the collision rate depends only weakly on cluster size, the maximum of the distribution $1/(\beta_{1,n} c_{n,0})$ likely coincides with the maximum of the energy barrier at the critical cluster size.

Similar arguments relying on the law of mass action and involving some approximations have been used (McGraw & Zhang, 2008) to motivate the multi-component nucleation theorem

$$\left(\frac{\partial \log J}{\partial \log C_i} \right)_{T, C_{j \neq i}} = n_i^* + \epsilon_i, \tag{7}$$

where C_i is the monomer concentration of component i (in a multi-component system, we use capital C_i for monomers of different types to distinguish from the cluster concentrations denoted by c_i), n_i^* is the number of molecules i in the critical cluster and ϵ_i gives the relative fraction of the growth flux out of the critical cluster due to addition of a molecule of type i, $\sum_i \epsilon_i = 1$.

In a case where clusters grow and decay only through additions and removals of single molecules, and all growth and evaporation processes occur along a single pathway, the multi-component nucleation theorem can also be derived rigorously. The derivation follows closely that of the single-component case, except that each growth step on the formation pathway is associated with the specific molecule type added to the cluster at that step. The net flux between two consecutive cluster sizes is now

$$I_k = \beta_{m_k,k} C_{m_k} c_k - \gamma_{m_k,k} c_{k+1},$$

where c_k and c_{k+1} are the concentrations of the kth and $(k+1)$th clusters, respectively, and m_k is the monomer type added to the cluster k to form the cluster $k+1$. Analogously to the one-component case, the birth-death equations can be rearranged as

Table 1
Assumptions used when deriving the nucleation theorem (A–D, I) and applying it to experimental results (E–H), their validity in different situations, and sections of this work where the validity is discussed in detail.

	Assumption	Validity	Discussion
A	The ΔG surface has one high energy barrier	Unknown	Sections 4.1, 4.2
B	Only monomer processes are relevant	Good (e.g. water nucleation)/ unknown (e.g. acid-base clustering)	Section 4.2
C	There are no external losses	Poor	Section 4.3
D	Multi-component nucleation proceeds along a single pathway	Unknown	Sections 4.1, 4.5
E	The nucleation rate with respect to vapor concentrations can be obtained from measurements	Poor (atmosphere)/unknown (experiments)	Sections 4.4, 4.7 Korhonen et al. (2011)
F	The system is in steady-state	Unknown (atmosphere)/good (chamber experiments)/poor (flow tube)	Section 4.6
G	All other conditions are kept constant	Poor (atmosphere, flow tube)/good (chamber experiments)	Sections 4.5, 4.7
H	The partial derivative (Eq. (7)) can be accurately determined	Poor	Sections 4.1, 4.4, 4.7
I	Collision and evaporation rates are connected by detailed balance	Unknown	

$I_k/(\beta_{m_k,k}\, C_{m_k} c_{k,0}) = c_k/c_{k,0} - c_{k+1}/c_{k+1,0}$ and summed to give

$$J = \left(\sum_{k=1}^{\infty} \frac{1}{\beta_{m_k,k} C_{m_k} c_{k,0}} \right)^{-1}. \tag{8}$$

The constrained equilibrium cluster concentrations have again a power-law dependence on monomer concentrations, $c_{k,0} \propto \prod_{i=1}^{M} C_i^{n_{k,i}}$ where M is the number of molecule types and the exponent $n_{k,i}$ is the number of molecules of species i in cluster k. The derivative corresponding to that of Eq. (5) depends on whether the monomer concentrations in the numerator and denominator correspond to the same molecule type:

$$\left(\frac{\partial (C_{m_k} c_{k,0})}{\partial C_i} \right)_{C_{j \neq i}} = (n_{k,i} + \delta_{m_k,i}) \frac{C_{m_k} c_{k,0}}{C_i},$$

where $\delta_{m_k,i}$ is the Kronecker delta ($\delta_{m_k,i} = 1$ if $m_k = i$ and $\delta_{m_k,i} = 0$ otherwise), and the derivative of the nucleation rate becomes

$$\left(\frac{\partial \log J}{\partial \log C_i} \right)_{T, C_{j \neq i}} = \frac{\sum_{k=1}^{\infty} \frac{n_{k,i} + \delta_{m_k,i}}{\beta_{m_k,k} C_{m_k} c_{k,0}}}{\sum_{l=1}^{\infty} \frac{1}{\beta_{m_l,l} C_{m_l} c_{l,0}}} \equiv \overline{n}_i + \overline{\epsilon}_i, \tag{9}$$

where the summations go over the clusters on the formation pathway. Once again, if the sum in the numerator is dominated by a sharp maximum in the distribution $1/(\beta_{m_k,k} C_{m_k} c_{k,0})$ at one cluster size k^*, $\overline{n}_i$ is close to the number of molecules i in that cluster. Similarly $\overline{\epsilon}_i$ is close to one if the next step on the formation pathway after the cluster k^* is an addition of molecule i and close to zero if it is an addition of some other molecule type. As opposed to the one-component system, however, the monomer concentrations do not cancel out in Eq. (9), and they may affect the values of $\overline{n}_i$ and $\overline{\epsilon}_i$ if different monomer types have very different concentrations.

The kinetic derivations presented above for the one-component and multi-component systems are very general in the sense that they do not (explicitly) assume anything about the cluster energies. They do, however, contain several other very restrictive assumptions, both related to their derivation and to their application to experimental data. These assumptions and their validity are summarized in Table 1. The widely established conception that the ΔG surface contains one maximum (assumption A) follows from thermodynamic treatment of a bulk liquid droplet, where the formation free energy of a cluster is the energy difference between the liquid and vapor phases minus the energy required to form the surface separating the phases. The birth-death equations are derived assuming that the growth and decay of the clusters occurs via a Szilárd-Farkas scheme, that is solely via monomer collisions and evaporations, and that there are no external loss terms such as deposition of clusters on surfaces or coagulation with larger particles (assumptions B and C). Assumption D (single nucleation pathway) is required for the present derivation of the multi-component nucleation theorem, but is not based on any prior evidence. Assumptions E–H are essentially related to the experimental conditions, measurement accuracy and data analysis. It is assumed that the flux from the critical cluster to larger sizes can be obtained from the observed appearance rate of freshly formed particles at some larger size (assumption E). Concentrations of all precursor vapors and clusters, and all ambient conditions such as temperature, must be constant during the particle formation event (assumptions F and G). Finally, the formation free energies ΔG_n, and thus also the composition of the critical cluster, or equivalently the slope of the particle formation rate as a function of the concentration of any component i (right-hand side of Eq. (7)), depend on the monomer concentrations. Therefore application of the first nucleation theorem to experimental data also requires the resolution and accuracy of the data to be sufficient for determining the partial derivative (left-hand side of Eq. (7)) as a function of the monomer concentration (assumption H).

For a multi-component system, the nucleation theorem may not be applicable even in the case where all the assumptions of Table 1 are valid, if the traditional definition of the critical cluster being located at the saddle point of the ΔG surface is used. As the frequency at which a molecule collides with a cluster depends on the concentration of the molecule, components with a high concentration collide with the clusters more often than components with a lower concentration. As a result, the flux may be distorted from the energetically optimal growth pathway, and does not necessarily proceed via the saddle point of the free energy surface at all. Thus, the energy barriers related to cluster formation may be higher than would be expected based on the saddle point of the formation free energy surface, and can only be solved by taking explicitly into account the actual growth pathway (Li et al., 2000; Wyslouzil & Wilemski 1995, 1996). The nucleation rate, on the other hand, is related by Eq. (9) to the composition of the cluster(s) on the formation pathway with the highest ΔG value(s). This disparity can, however, easily be resolved by redefining the critical cluster as the highest-energy cluster on the formation pathway, and we use this new definition in the rest of this paper.

When ions are present, cluster formation can proceed along three separate ΔG surfaces corresponding to neutral, negatively charged and positively charged clusters. Furthermore, clusters can move from one charging state to another at any size by collisions with ions or charged clusters (Olenius et al., 2013a). In the atmosphere, ions originate from cosmic rays and radon decay, and while their formation rate and total concentration are relatively constant, the concentrations of individual molecular ions vary. For instance, the concentration of the bisulfate ion (HSO_4^-), the ionic monomer relevant for the nucleation theorem, depends on the sulfuric acid concentration (Olenius et al., 2013b). Therefore, if the nucleation rate in the presence of natural ionization is measured at different sulfuric acid concentrations, the bisulfate ion concentration is not constant between the measurements, and thus assumption G does not hold and the nucleation theorem cannot be used.

The derivation of the nucleation theorem assumes that evaporation rates

$$\gamma_{1,k} \propto \beta_{1,k} \exp\left(\frac{\Delta G_{k+1} - \Delta G_k}{k_B T}\right) \tag{10}$$

are connected to collision rates and cluster formation energies by detailed balance (assumption I). It is also implicitly assumed that each number of molecules (or in the multi-component case each set of numbers of different molecules) corresponds to exactly one cluster energy and that the configuration corresponding to that energy is reached immediately when the cluster is formed. This simplified view is, however, probably not correct. Especially in the case of large asymmetrical molecules, it is more likely that the colliding molecules or clusters first stick together in a configuration determined by the collision geometry and then gradually rearrange to an energetically more favorable configuration. Evaporation of the cluster would then be more probable shortly after it is formed than once it has found a more stable configuration. The effect of excess energy released when a cluster is formed is also neglected, which is supported by earlier studies suggesting that atmospherically relevant clusters have enough vibrational degrees of freedom to accommodate most of the collision energy (Kurtén et al., 2010), and that the corresponding increase in cluster temperature is not likely to increase the evaporation rates to the extent that the derivative $\partial(\log J)/\partial(\log C)$ is affected strongly (Barrett, 2008). However, there is at present no other way to obtain cluster evaporation rates than to make these simplifications and use Eq. (10), although the first steps toward a more detailed description have recently been taken (Loukonen et al., 2014a,b). Therefore assessing the effect of assumption I on the nucleation theorem is beyond the scope of this study.

3. Methods

3.1. ACDC

We simulated the formation of sulfuric acid (H_2SO_4)–ammonia (NH_3) and sulfuric acid–dimethylamine ($(CH_3)_2NH$, or shortly DMA) clusters with a dynamic cluster model ACDC (Atmospheric Cluster Dynamics Code; McGrath et al., 2012; Olenius et al., 2013a). ACDC generates the equations for the time derivatives of the concentrations of a given set of clusters, also called the cluster birth-death equations or Becker-Döring equations, and solves the time evolution of the concentrations by numerical integration using the Matlab ode15s solver (Shampine & Reichelt, 1997). If evaporation is disabled for all cluster sizes, the set of equations to be solved reduces to the Smoluchowski coagulation equations. In addition to monomer collisions and evaporations, the code enables the inclusion of external sink and source terms for all cluster sizes and all possible cluster-cluster collision and fragmentation processes. If the system also contains electrically charged clusters, the equations include ionization and recombination by generic ionizing species that give their charge to other molecules and clusters upon collisions but do not otherwise participate in cluster formation (see Olenius et al., 2013a or Almeida et al., 2013 for more details). Vapor (monomer) concentrations can either be set to a predetermined value or solved from the birth-death equations when source terms and initial monomer concentrations are given.

For collisions between electrically neutral clusters, the collision coefficients are calculated as hard-sphere collision rates, and for collisions between a neutral and an ionic cluster, a parameterization based on the cluster masses and the dipole moment and polarizability of the neutral cluster (Su & Chesnavich, 1982) is used. The evaporation coefficients are calculated from quantum chemical Gibbs free energies of formation according to the condition of detailed balance (Eq. (10)) as described by Ortega et al. (2012).

The particle formation rate is defined in ACDC as the rate at which clusters grow out of the simulation system. To account for the limited size of the system (the largest clusters are $(H_2SO_4)_5 \cdot (NH_3)_5$ and $(H_2SO_4)_4 \cdot ((CH_3)_2NH)_4$), clusters are only

allowed to leave the system if they have a favorable composition, or in practice an acid:base ratio of approximately one (neutral clusters must contain at least 6 H_2SO_4 molecules + 5 NH_3 molecules, 5 H_2SO_4 molecules + 4 DMA molecules, 4 H_2SO_4 molecules + 5 DMA molecules, or in Section 4.6 5 H_2SO_4 molecules + 4 base molecules or 4 H_2SO_4 molecules + 5 DMA molecules, negatively charged clusters must have at least 1 HSO_4^- ion + 5 H_2SO_4 molecules + 1 NH_3 molecule, and positively charged clusters at least 1 NH_4^+ ion + 5 H_2SO_4 molecules + 5 NH_3 molecules). In the context of ACDC simulations, J always refers to this particle formation rate, not the nucleation rate at the critical size. The time evolution of the cluster concentrations and the particle formation rate are obtained directly as output from the integration of the birth-death equations, and the steady-state formation rate can be solved by setting the vapor concentrations or their source terms to a constant value and running the simulation until all concentrations have reached a constant value.

Water vapor and the hydration of clusters are not taken into account in this study due to the lack of thermochemical data for hydrated clusters. The presented formation rates should therefore not be interpreted as quantitative predictions. Instead, the systems of dry clusters should be considered as a simplified test case for examining the performance of the nucleation theorem.

In this study, ACDC was used to solve the particle formation rate in two- and three-component sulfuric acid–base systems, where the base is either ammonia, dimethylamine (DMA) or both. The temperature was 278 K in all simulations. In Sections 4.3 and 4.6 we used for all clusters a loss term $-L \times c_i$ where L is a size-independent loss constant corresponding to coagulation with larger particles or deposition on walls and c_i is the cluster concentration. The simulation results should again be interpreted as giving a qualitative estimate of the effect of losses. In reality, the loss coefficients depend on cluster size, and in case of coagulational losses to larger particles also on the time evolution of the particle distribution. Detailed information on the clusters included in the systems and on the boundary conditions, and the quantum chemical data can be found in our earlier publications (Almeida et al., 2013; Olenius et al., 2013a). Both ammonia and DMA have been observed in the atmosphere in various urban and rural areas (Ge et al., 2011), and our simulations were performed at realistic ambient sulfuric acid and base concentrations that produce particle formation rates comparable to those observed in the atmosphere, both according to ACDC simulations and chamber experiments (Almeida et al., 2013; Kirkby et al., 2011).

To study the dependence of the particle formation rate on precursor concentrations, we ran each simulation at several sulfuric acid concentrations and two base concentrations (or vice versa in the lower panel of Fig. 4), and approximated the partial derivative based on the difference between the formation rate at two adjacent simulation points as

$$\left(\frac{\partial \log J}{\partial \log C_i}\right)_{T,C_{j\neq i}} \approx \left(\frac{\Delta \log J}{\Delta \log C_i}\right)_{T,C_{j\neq i}},$$

where C_i is the acid or the base concentration. The step size along the logarithmic concentration axis was set to 20 simulation points per an order of magnitude, and the concentrations of the other compound were set to $1\times[C_j]$ and $1.01\times[C_j]$, except in Fig. 8 we used 10 simulation points per an order of magnitude for the sulfuric acid concentration and a base concentration $1.1\times$[base]. The Gibbs free energy of formation as a function of cluster growth was determined by tracing the growth pathways as described by Olenius et al. (2013a). In the case that the main growth route exhibits one or more energy barriers, the critical cluster was identified as the location of the highest barrier.

3.2. UHMA

In addition to the cluster kinetics model, we used an aerosol microphysics model to investigate the applicability of the nucleation theorem to interpret field data. Our aerosol microphysics model UHMA (University of Helsinki Multicomponent Aerosol model; Korhonen et al., 2004, 2011) was used to generate synthetic size distribution evolution data that resembles what is measured during atmospheric particle formation events. A detailed description of the model and the data analysis scheme is given by Korhonen et al. (2011) (see also Sihto et al., 2006), and we present here only the details that differ from that study.

In the simulations, particles were assumed to nucleate at 1.5 nm and the nucleation rate was assumed proportional to the sulfuric acid concentration squared, i.e. $J_{1.5} = K[H_2SO_4]^2$. The time dependence of the sulfuric acid concentration was set to be parabolic, with a peak concentration of 1.5×10^6 cm^{-3} at noon and zero values before 10 am and after 2 pm, and some random noise was added to mimic rapidly varying atmospheric conditions. (This time interval is somewhat shorter than what is seen in the atmosphere, and was chosen for computational reasons.) The value of K was taken randomly from a uniform distribution in the range 5×10^{-18} to 5×10^{-17} at each time step.

The cluster growth rates were prescribed (i.e. not calculated from simulated vapor concentrations) to be linearly dependent on cluster size, as indicated by recent atmospheric observations (Kuang et al., 2012). At the beginning of each simulation, the growth rates at 1.5 nm and 3 nm were selected from the ranges 0.4–1.4 and 1.4–2.4 nm/h, respectively, and the same growth rates were used for the length of the simulation. This assumption of sulfuric acid-independent growth rates mimics a situation where the newly formed particles grow mainly by oxidized organic compounds.

The evolution of the particle size distribution was modeled using a fully moving sectional grid. The number of size bins was 20 at the beginning of the simulation, and new bins were created for the freshly nucleated particles, leading to a total of 260 bins at the end of the run. The time step was 0.2 s when sub-4-nm particles were present, and 60 s otherwise. The pre-existing aerosol population at the beginning of the run was modeled as one narrow mode at 200 nm in diameter corresponding to a coagulation sink between 0.04×10^{-3} and 0.11×10^{-3} s^{-1}. The sulfuric acid concentration and the particle size distribution above 3 nm diameter were stored for analysis every 10 min.

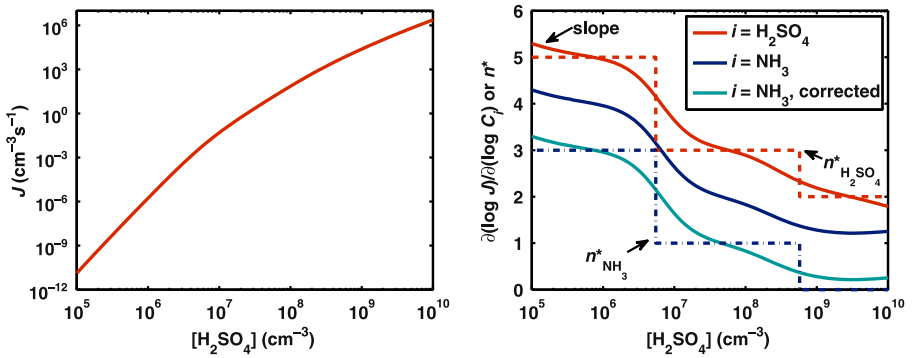

Fig. 1. Left panel: particle formation rate as a function of H_2SO_4 monomer concentration at 278 K and $[NH_3]=10$ ppt. Right panel: logarithmic partial derivatives of the particle formation rate with respect to the sulfuric acid (red solid line) and ammonia (dark blue solid line) monomer concentrations, the ammonia derivative corrected with $\epsilon_{NH_3}=1$ (light blue solid line), and the number of sulfuric acid (red dashed line) and ammonia (dark blue dash-dotted line) molecules in the critical cluster, defined here as the highest energy barrier on the main growth pathway. (For interpretation of the references to color in this figure caption, the reader is referred to the web version of this paper.)

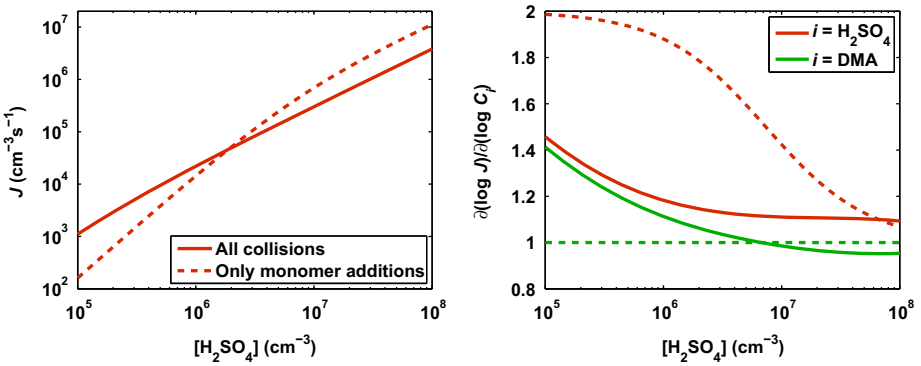

Fig. 2. Left panel: neutral particle formation rate at $[DMA]=10$ ppt. Right panel: logarithmic partial derivatives of the formation rate with respect to the sulfuric acid (red) and DMA (green) monomer concentrations. Cluster-cluster collisions and fragmentations are either allowed (solid lines) or disabled (dashed lines). (For interpretation of the references to color in this figure caption, the reader is referred to the web version of this paper.)

4. Case studies

In this section we go through the assumptions listed in Table 1 and present examples where they may lead to a wrong assignment of the critical cluster. Results from ACDC are presented in Sections 4.1–4.6, and results from UHMA in Section 4.7. Sections 4.1–4.3 discuss the assumptions used in the derivation of nucleation theorem, while Sections 4.4–4.6 consider issues related to precursor vapor concentrations and Section 4.7 focuses on difficulties in extracting the nucleation rate from measurements.

4.1. The critical cluster size depends on conditions (assumptions A, D and H)

According to the quantum chemical cluster formation energies used in this study, neutral sulfuric acid–ammonia cluster formation proceeds along a pathway containing three local maxima (Olenius et al., 2013a). Depending on the precursor concentrations, any one of the clusters $(H_2SO_4)_5\cdot(NH_3)_3$, $(H_2SO_4)_3\cdot NH_3$ or $(H_2SO_4)_2$ can correspond to the highest maximum, and thus be the rate limiting critical cluster.

Figure 1 presents the particle formation rate and its logarithmic partial derivatives over a wide range of sulfuric acid concentrations. The slope of the particle formation rate with respect to the sulfuric acid concentration is high at low $[H_2SO_4]$ and decreases with increasing $[H_2SO_4]$. A comparison to the critical cluster composition shows that the slope $\partial(\log J)/\partial(\log[H_2SO_4])$ corresponds closely to the number of sulfuric acid molecules in the critical cluster. However, while the identity of the critical cluster changes in discrete steps, the slope decreases smoothly. This can easily be understood from Eq. (6): the nucleation theorem assumes that the critical cluster size alone determines the slope, but in this case the two highest maxima of the ΔG curve both contribute significantly to the summation of Eq. (9) near the transition from one critical cluster to the other.

Examining the main growth pathway in this system (Olenius et al., 2013a), it can be seen that the next step on the growth pathway after each local maximum is the addition of an ammonia molecule. Therefore, in all conditions considered in Fig. 1, the flux across the critical cluster is in the direction of the ammonia coordinate, and the correction terms of Eq. (7)

are $\epsilon_{H_2SO_4} = 0$ and $\epsilon_{NH_3} = 1$. Taking the correction term into account, the nucleation theorem is also approximately valid for the ammonia derivative. The interpretation and validity of Eq. (9) are discussed in more detail in Section A.1 of the Appendix.

In the case of experimental data, the growth pathway is not known. Since the correction terms ϵ_i depend on what is the next step after passing the critical size, they can at best be guessed based on precursor concentrations but not determined reliably. If the critical cluster is small, this leads to a significant uncertainty in determining its composition, although the total number of molecules can in principle be solved as the sum of the correction terms is always one. Making a single linear fit to a set of measurements where the critical cluster varies from point to point will also lead to an incorrect attribution of the critical cluster.

4.2. Cluster-cluster collisions (assumptions A and B)

In the presence of a strong base, such as DMA, small strongly bound acid-base clusters may be abundant enough to contribute significantly to cluster growth (Olenius et al., 2013a; see also Vehkamäki et al., 2012). Figure 2 shows the formation rates and their slopes at [DMA] = 10 ppt both in a simulation where only monomer collisions and evaporations are considered, and in a simulation where cluster-cluster processes are included. Depending on the H_2SO_4 concentration, the formation rate of the case where only monomer processes are included can be either lower or higher than in the case where all possible processes are taken into account. When cluster-cluster collisions are allowed, they contribute significantly to the growth, and as the growth rate is higher, cluster concentrations are lower (see Section A.2 of the Appendix). The formation rate of clusters of a certain size depends both on the concentration of smaller clusters and on their growth rate; at low acid concentrations the effect of the growth rate dominates and the formation rate is higher when all collisions are allowed, and at higher acid concentrations the effect of cluster concentrations dominates. It should be noted, however, that forbidding cluster-cluster collisions is only a hypothetical tool for understanding how they affect the formation rate, and that there is no reason to believe that cluster-cluster collisions would not contribute to particle formation in reality if cluster concentrations are significant compared to monomer concentrations. Based on the cluster energies, fragmentation rates of clusters into two smaller clusters may in some cases be comparable to monomer evaporation rates. Fragmentation was allowed when cluster-cluster collisions were also allowed and forbidden when they were not. However, from the simulations, it was observed that the fragmentation processes had little effect on the particle formation rate. In the case where cluster-cluster collisions were enabled, disabling fragmentation changed the particle formation rate at most less than 0.25%.

In situations where small clusters are abundant and cluster-cluster collisions cannot be neglected, the derivation of the nucleation theorem is not valid and the slope of the formation rate does not, even in principle, give information on the critical size. This is the case when formation of the smallest clusters is energetically favorable. If there is no energetic barrier and no critical cluster at larger sizes, the particle formation rate is approximately proportional to the precursor concentrations, and the slopes are close to one in accordance to the nucleation theorem. If, on the other hand, there is a critical cluster at some larger size, the nucleation theorem is not valid (Vehkamäki et al., 2012).

In conditions of Fig. 2, cluster formation is barrierless, partly because energy barriers are avoided by collisions with small clusters instead of subsequent additions of monomers. If, on the other hand, only monomer collisions are allowed, the energy profile along the formation pathway has a local maximum at the cluster size $(H_2SO_4)_3 \cdot (DMA)_2$. However, as this is not a global maximum but instead has a negative formation free energy compared to monomers, its location cannot be inferred by slope analysis from Fig. 2.

4.3. External losses (assumption C)

When particles are forming, growth and evaporation are usually not the only processes at play as assumed in the nucleation theorem. Instead, the clusters may be lost by coagulating onto larger particles or, in laboratory experiments, by depositing to walls before they reach a detectable size. The effect of these external losses is strongest when cluster formation and early growth are slow compared to the loss rate. The flux between consecutive clusters k and $k+1$ can still be written according to Eq. (2) as $I_k = \beta_{1,k} c_1 c_k - \gamma_{1,k} c_{k+1}$, but the steady-state flux is no longer equal for different cluster sizes k as some of the clusters are lost on the way. The cluster concentrations are overall lower than in the absence of losses, and the relative difference increases with cluster size as more clusters are lost at each growth step. Therefore, both the forward and backward fluxes are lowered compared to the loss-free case. For each pair of consecutive clusters, the relative decrease in concentration is larger for the bigger cluster, and thus the backward flux is lowered relatively more than the corresponding forward flux. As a consequence, at small sizes where evaporation is important, the net flux increases, and at larger sizes where evaporation is negligible the net flux decreases.

In experimental studies, formation rates are typically evaluated at a diameter larger than the critical cluster size, and we focus here on such a case. We also assume that the external losses are independent of the precursor concentration and particle formation rate, which is mostly relevant for chamber experiments where deposition to walls is the major loss mechanism. An increase in precursor concentrations then typically increases the particle formation rate both directly and by increasing the growth rate and thus reducing the relative effect of losses, and thus the slope of the formation rate with respect to vapor concentrations is higher than in the absence of losses. In a (pseudo-)one-component case the situation is

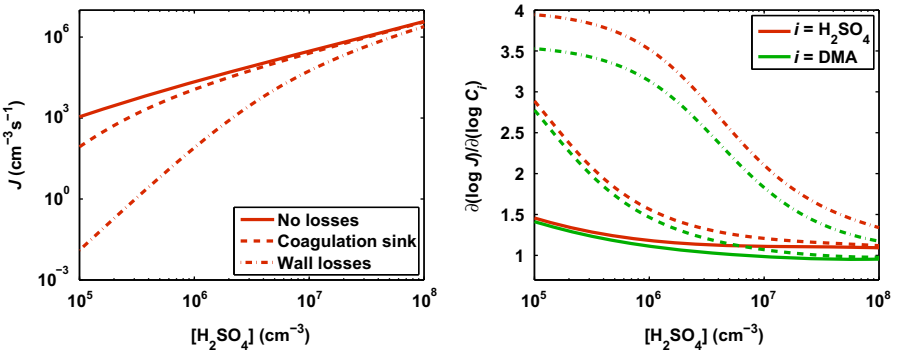

Fig. 3. Left panel: neutral particle formation rate at [DMA]=10 ppt with no external losses (solid line), with a coagulation loss coefficient $2.6 \times 10^{-3}\ s^{-1}$ corresponding to the Hyytiälä boreal forest station (Dal Maso et al., 2008) (dashed line) and with a wall loss coefficient $2.3 \times 10^{-2}\ s^{-1}$ corresponding to the *IfT*-LFT flow tube (Berndt and Richters, 2012) (dash-dotted line). Right panel: logarithmic partial derivatives of the formation rate with respect to the sulfuric acid (red) and DMA (green) monomer concentrations. (For interpretation of the references to color in this figure caption, the reader is referred to the web version of this paper.)

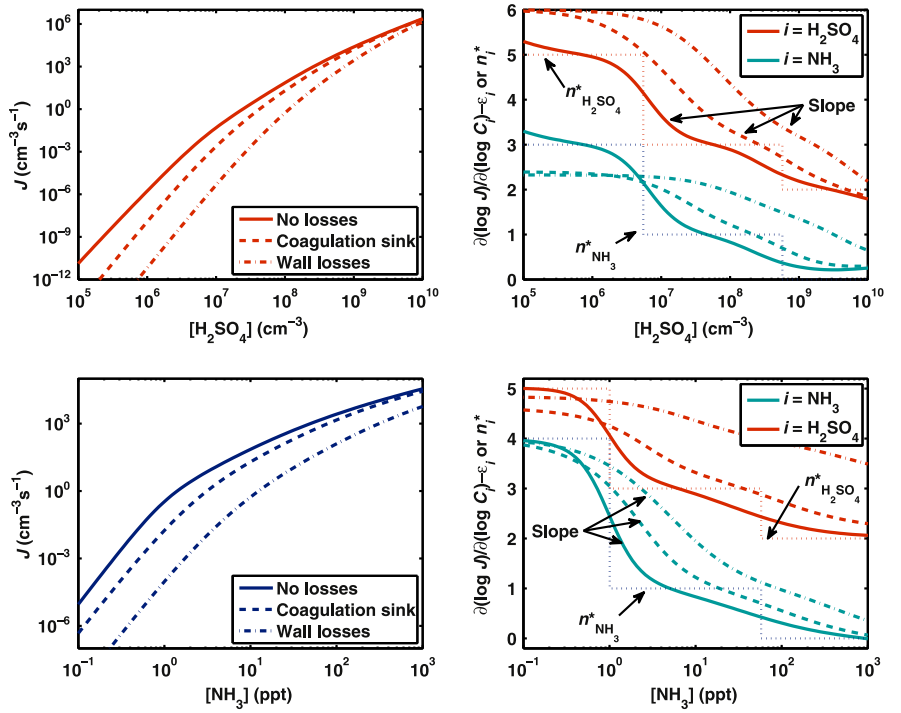

Fig. 4. Upper left panel: Neutral particle formation rate at [NH_3]=10 ppt with no external losses (solid line), with a coagulation loss coefficient $2.6 \times 10^{-3}\ s^{-1}$ corresponding to the Hyytiälä boreal forest station (Dal Maso et al., 2008) (dashed line) and with a wall loss coefficient $2.3 \times 10^{-2}\ s^{-1}$ corresponding to the *IfT*-LFT flow tube (Berndt & Richters, 2012) (dash-dotted line). Upper right panel: Logarithmic partial derivatives of the formation rate with respect to the sulfuric acid (red solid, dashed and dash-dotted lines) and ammonia (light blue lines) monomer concentrations, where the ammonia derivative is corrected by subtracting $\epsilon_{NH_3} = 1$. Lower panels: same as the upper panels but with a constant sulfuric acid concentration of $10^7\ cm^{-3}$ and a varying ammonia concentration. (For interpretation of the references to color in this figure caption, the reader is referred to the web version of this paper.)

straight-forward, and the effect of losses has been studied previously for binary H_2SO_4-H_2O nucleation (Ehrhart & Curtius, 2013) and can even be treated analytically (Malila et al., 2014, note that the earlier version in Malila et al., 2011, 2013 had an error). In a multi-component system, on the other hand, the presence of several molecule types with possibly very different monomer concentrations, as well as potential competition between different formation pathways, complicates the situation and the effect of losses on the slope is not as straight-forward.

Figure 3 shows the effect of external losses on the behavior of the steady-state formation rate in the sulfuric acid–DMA system. The losses were modeled using a size-independent loss constant of either $2.6 \times 10^{-3}\ s^{-1}$ or $2.3 \times 10^{-2}\ s^{-1}$ corresponding to coagulation losses at the Hyytiälä boreal forest station (Dal Maso et al., 2008) and wall losses in the *IfT*-LFT flow tube (Berndt & Richters, 2012), respectively. It should be noted that the simulations do not aim to mimic atmospheric conditions or a flow tube experiment, but only to probe the effect of losses of different magnitudes in an otherwise ideal system.

As stated above, at $T=278$ K and [DMA] = 10 ppt there is no critical cluster in the sulfuric acid–DMA system. However, in the presence of wall losses, the slopes can be close to four for both sulfuric acid and DMA, which the nucleation theorem would interpret as a critical cluster of seven molecules in total, taking into account the correction terms ϵ_i which sum up to one. Corresponding results for the sulfuric acid–ammonia system are presented in the upper panels of Fig. 4. Also in this case the losses lower the formation rate and increase its slope with respect to sulfuric acid. However, at low sulfuric acid concentrations when the ammonia concentration is substantially higher than the acid monomer concentration, the relative effect of losses increases with increasing ammonia concentration and the slope of the formation rate with respect to ammonia is lower than in a loss-free case. At lower ammonia concentrations when $[H_2SO_4] \gg [NH_3]$ (lower panel of Fig. 4) losses reduce the slope of the formation rate with respect to both sulfuric acid and ammonia concentrations. External losses do not affect the cluster energetics, and in both of these examples the main growth pathway also remains unaltered. Therefore the identity of the critical cluster is not affected by losses while the slopes change considerably, implying that the nucleation theorem is no longer applicable when loss terms are allowed. In a multi-component system, the slope determined from formation rates measured above the critical size can be either increased or decreased by losses, and the nucleation theorem does not even give an upper or lower limit to the critical cluster size. In field observations, the coagulation sink varies between measurements, and no general conclusions about losses can be made. Clusters can also coagulate with freshly formed particles, complicating the situation further, and the effect of this process on the slope of the formation rate is discussed in Section 4.7.

4.4. Definition of the precursor concentration (assumptions E and H)

The sulfuric acid concentration is usually measured with a Chemical Ionization Mass Spectrometer (CIMS), which charges sulfuric acid molecules with nitrate ions and then detects them by mass spectrometry. However, the CIMS most probably also ionizes acid hydrates $H_2SO_4 \cdot (H_2O)_n$, acid-base clusters $H_2SO_4 \cdot (\text{base})_m$ and hydrated acid-base clusters $H_2SO_4 \cdot (\text{base})_m \cdot (H_2O)_n$ (Eisele & Tanner, 1993; Hanson & Eisele, 2000; Kupiainen-Määttä et al., 2013), and after ionization the water and/or base molecules are lost. Consequently, the signal due to pure H_2SO_4 monomers is indistinguishable from the signal due to other clusters containing one sulfuric acid molecule, and the measured sulfuric acid concentration is not equal to the monomer concentration relevant to the nucleation theorem if cluster concentrations are non-negligible. Our quantum chemical calculations indicate that $H_2SO_4 \cdot$ DMA clusters are very strongly bound and have significant concentrations even at ppt-level base concentrations, but some other theoretical studies have predicted significantly weaker binding (Leverentz et al., 2013; Nadykto et al., 2011). Experiments have not yet provided conclusive results regarding the abundance of $H_2SO_4 \cdot$ base dimers, but the recent results of Almeida et al. (2013) show that the presence of DMA increases substantially the concentration of clusters containing two H_2SO_4 molecules. On the other hand, it is well-known that H_2SO_4 molecules form hydrates at ambient relative humidities (Hanson & Eisele, 2000), and the CIMS is also assumed to detect $H_2SO_4 \cdot (H_2O)_n$ clusters as pure H_2SO_4 vapor. Therefore the conclusions of this section are also relevant for all sulfuric acid nucleation measurements in the presence of water.

The effect of the "definition" of the sulfuric acid concentration (whether only monomers or also acid molecules bound to other compounds are counted) is illustrated in Fig. 5 for the sulfuric acid–DMA system. In the left panel, the solid line presents the particle formation rate as a function of sulfuric acid monomer concentration, and the dashed line as a function of the CIMS-measurable sulfuric acid concentration $[H_2SO_4]+[H_2SO_4 \cdot \text{DMA}]$. At low sulfuric acid concentrations, most of the sulfuric acid is bound to DMA, but as the overall concentration increases, the fraction bound to DMA decreases. Consequently, the dashed line is shifted strongly to the right at low concentrations and somewhat less at higher concentrations, and its slope is therefore higher than for the solid line. After the formation of the $H_2SO_4 \cdot$ DMA cluster, the next few steps proceed by collisions with other $H_2SO_4 \cdot$ DMA clusters, and the process is in practice kinetically limited

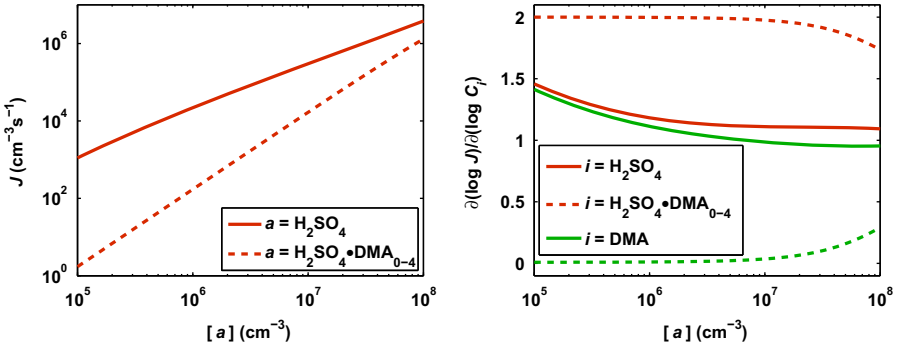

Fig. 5. Left panel: neutral particle formation rate at [DMA] = 10 ppt. Right panel: logarithmic partial derivatives of the formation rate with respect to the sulfuric acid (red) and DMA (green) concentrations. The sulfuric acid concentration is either the monomer concentration (solid lines) or the measurable concentration $\sum_{d=0}^{4}[H_2SO_4 \cdot (DMA)_d]$ (dashed lines). (For interpretation of the references to color in this figure caption, the reader is referred to the web version of this paper.)

barrierless one-component condensation of $H_2SO_4 \cdot DMA$ with a particle formation rate corresponding to the collision rate of two such units. Since the CIMS-measurable sulfuric acid concentration $[H_2SO_4]+[H_2SO_4 \cdot DMA]$ is dominated by the cluster concentration $[H_2SO_4 \cdot DMA]$ except at very high H_2SO_4 concentrations, the slope of the particle formation rate with respect to this concentration is 2 and there is no DMA dependence. This is in agreement with the nucleation theorem if the critical cluster in barrierless coagulation is defined to be the monomer (as is usually done), but the correct interpretation is only possible if it is known that all measured H_2SO_4 molecules are bound to DMA. In practice, the distribution of H_2SO_4 monomers and different clusters containing one H_2SO_4 molecule is not known, and thus the application and the interpretation of the nucleation theorem are not possible.

4.5. Presence of ions (assumptions B, D and G)

Electrically charged molecules and clusters are produced in the atmosphere by ionization due to galactic cosmic rays and radon decay. Ionic clusters are able to enhance particle formation as they are strongly bound by electrostatic forces. In the presence of other enhancing species, such as bases, the contribution of ions to the particle formation rate depends on the relative enhancement due to these other species. In the sulfuric acid–DMA system at [DMA] = 10 ppt (not shown) the effect of ions on the particle formation rate (and thus its slope) in the studied $[H_2SO_4]$ range is negligible, as DMA has a significant enhancing effect on the binding and growth of neutral sulfuric acid clusters, resulting in the role of ions being minor overall (Almeida et al., 2013).

In the sulfuric acid–ammonia system, on the other hand, ions have a strong enhancing effect on particle formation at low sulfuric acid concentrations (Kirkby et al., 2011). The effect of an ion production rate of 3 ion pairs $cm^{-3}\,s^{-1}$, approximately the ionization rate in the atmospheric boundary layer (Kirkby et al., 2011), is shown in Fig. 6. The corresponding HSO_4^- and NH_4^+ ion concentrations are presented in Fig. 13 of the Appendix. In this case, particle formation proceeds along numerous different pathways, but at low sulfuric acid concentrations the most important routes start by the formation of small positive and/or negative clusters, which then recombine to form larger neutral clusters and continue to grow by addition of H_2SO_4 and NH_3 monomers. An increase in the concentration of sulfuric acid or ammonia molecules leads to an increase in cluster formation, and therefore the logarithmic derivatives of J with respect to both monomer concentrations are positive.

The contribution of ions to particle formation can, however, never exceed the ion formation rate, and when this limit is approached, an increase in monomer concentrations no longer increases the ion-mediated particle formation rate. This is seen as a flattening of the J curve and a dip in the derivatives in Fig. 6. When the sulfuric acid concentration is further increased, neutral cluster formation starts to dominate over the ion-induced pathways, and the derivatives of J increase again to join those of the purely neutral case.

All clusters along the growth pathways within the negative and positive charging states have a negative formation free energy with respect to the HSO_4^- and NH_4^+ ions, respectively, but both formation pathways have local energy barriers at larger sizes. It is, however, impossible to extract the absence of a barrier in charged cluster formation or the size and composition of the neutral critical cluster from the slope of the formation rate. This results from the violation of three assumptions of the nucleation theorem: the ion monomer concentrations are not constant (G), particle formation proceeds along several pathways (D) and cluster-cluster collisions are non-negligible (B). As a comparison, Fig. 6 also presents the particle formation rate in a case where only negative clusters are present and the bisulfate ion concentration is set to a constant value corresponding to the maximum bisulfate ion concentration in the case with a constant ion pair production rate. In this case, particle formation starts by the collision of a HSO_4^- ion and a H_2SO_4 molecule and proceeds along a single pathway by additions of H_2SO_4 and NH_3 monomers. Accordingly, the logarithmic derivatives of J with respect to monomer

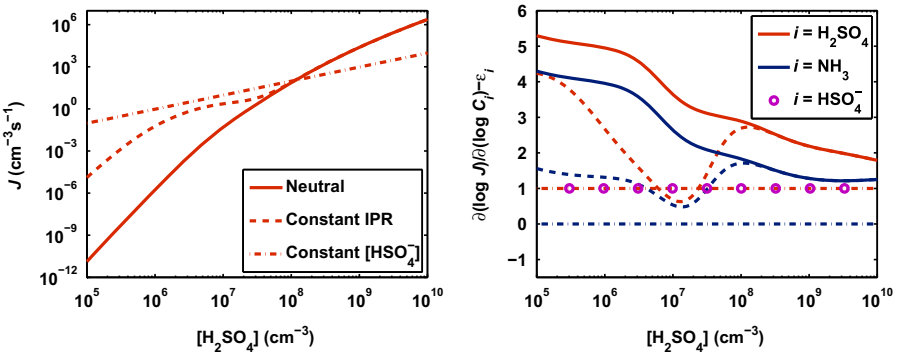

Fig. 6. Left panel: total particle formation rate at $[NH_3] = 10$ ppt in systems containing only neutral clusters (solid line), neutral as well as positively and negatively charged clusters with an ion pair production rate IPR = 3 $cm^{-3}\,s^{-1}$ (dashed line) and only neutral molecules and negatively charged clusters with a constant HSO_4^- ion concentration of 427 cm^{-3} (dash-dotted line). Right panel: logarithmic partial derivatives of the formation rate with respect to the sulfuric acid (red), ammonia (blue) and, for the system with only negative clusters, bisulfate ion (purple circles) concentrations. (For interpretation of the references to color in this figure caption, the reader is referred to the web version of this paper.)

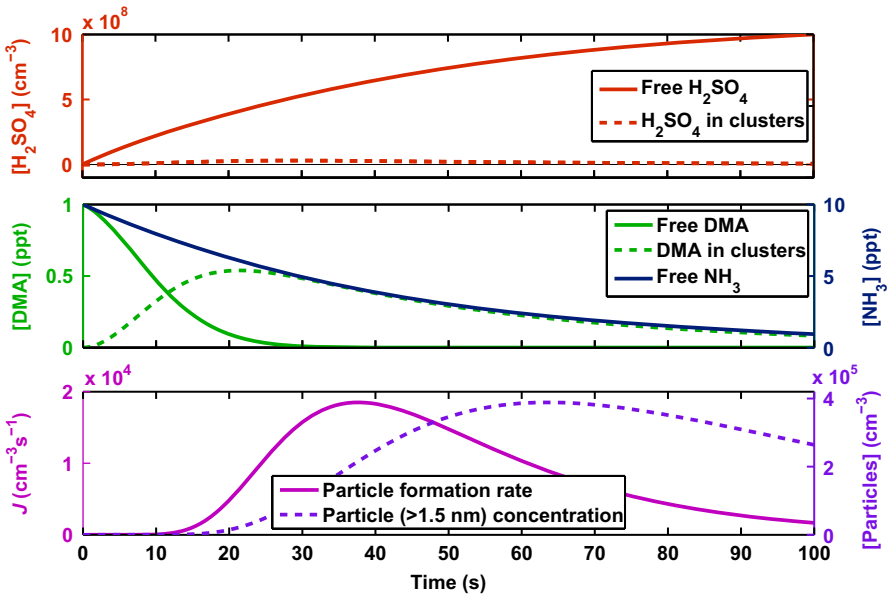

Fig. 7. Modeled precursor gas, cluster and particle concentrations in a flow tube experiment where sulfuric acid is produced *in situ* and the wall loss coefficient is $2.3 \times 10^{-2}\ s^{-1}$.

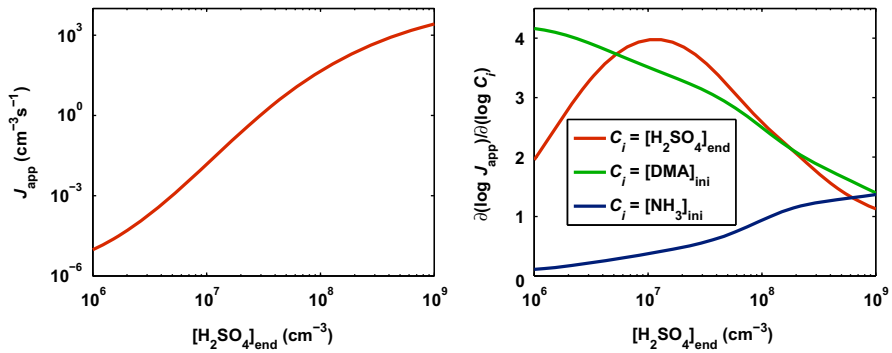

Fig. 8. Left panel: apparent particle formation rate in a flow tube, defined as the particle concentration at the end of the tube divided by the residence time, as a function of end sulfuric acid concentration and keeping the initial ammonia and DMA concentrations constant. Right panel: logarithmic partial derivatives of the particle formation rate with respect to the final sulfuric acid concentration and the initial ammonia and DMA concentrations.

concentrations are equal to one for sulfuric acid and the bisulfate ion and zero for ammonia, as the first collision is the rate limiting step and its product $H_2SO_4 \cdot HSO_4^-$ has a negligible evaporation rate.

4.6. *Experiments where concentrations are not constant (assumption F)*

The nucleation rate appearing in the nucleation theorem is a steady-state nucleation rate. Steady-state nucleation may indeed be achieved in a chamber experiment, although the nucleation rate is typically evaluated before the steady-state is reached. Atmospheric nucleation might also, at least in some cases, be close to a steady state. In flow tube experiments, however, a perfect steady-state cannot be achieved. Precursor gases can be introduced into the flow tube in two ways: either they are mixed into the carrier gas or they can be produced *in situ* inside the tube. The former method is used for water vapor, bases and organic compounds as well as impurities of the carrier air, while sulfuric acid is often produced in the tube from SO_2. In any case, the vapor concentrations are not constant along the length of the tube, and thus a parcel of gas traveling through the tube does not experience time-independent vapor concentrations, implying that cluster formation is not in a steady state.

An example of a flow tube experiment is presented in Fig. 7. The zero-dimensional simulation assumes that gases are locally well-mixed and concentrations depend only on the position along the length of the flow tube, or equivalently the time that it takes for the flow to reach that point. In reality, the concentrations also have radial gradients, but the zero-dimensional approach can be seen as an approximation for the situation at the axis of the flow tube (Becker & Reiss, 1976). At the beginning of the tube, sulfuric acid, ammonia and DMA concentrations are set to $10^6\ cm^{-3}$, 10 ppt and 1 ppt,

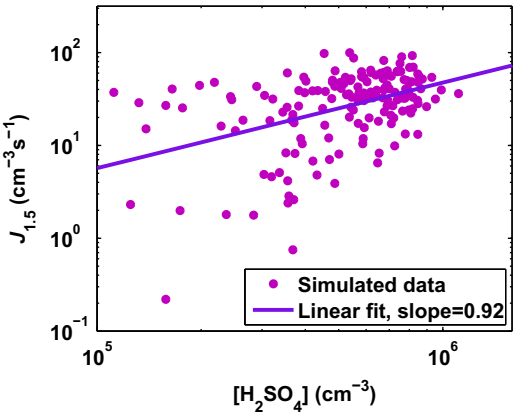

Fig. 9. Particle formation rates at 1.5 nm determined every 10 min for eight model runs of new-particle formation events as a function of sulfuric acid concentration. The linear least-squares fit to the data points has a slope of 0.92, while the input nucleation rate is of the form $J_{1.5} = K[H_2SO_4]^2$ corresponding to a slope of 2. Only data points for which the simulated sulfuric acid concentration was higher than 10^5 cm^{-3} are included (approximately the detection limit for atmospheric sulfuric acid measurements). If data points below this limit were included, the slope of the fitted line would be 0.33.

respectively. Sulfuric acid is produced at a constant rate and its concentration increases as a function of time, but the increase gradually levels off because of wall losses. The ammonia concentration decreases along the length of the tube due to wall losses, and the DMA monomer concentration decreases even more rapidly through the formation of sulfuric acid–DMA clusters. The particle formation rate increases at first as small clusters form and gradually grow to larger sizes, but starts then to decrease as DMA is depleted. Near the end of the flow tube, the concentration of formed particles also starts to decrease as losses dominate over the formation rate. As a result, the measured apparent particle formation rate J_{app}, defined as the particle concentration at the end of the tube divided by the residence time, depends strongly on the time evolution of the system. Since the nucleation theorem requires the system to be in steady-state, it should not be used for determining the critical cluster composition in a case such as this. The critical cluster cannot even be defined for a whole experiment, because its identity changes along the tube with the precursor concentrations. The left panel of Fig. 8 shows the apparent particle formation rate as a function of the sulfuric acid concentration at the end of the tube. The right panel shows the slope of J_{app} with respect to the end sulfuric acid concentration and the initial base concentrations. At low acid concentrations, the particle formation rate is mostly limited by the DMA being lost on walls, and therefore the formation rate has a high slope with respect to the DMA concentration. At higher acid concentrations, more particles have time to form before the DMA is lost to the walls, and the slope with respect to sulfuric acid increases. Finally, at very high sulfuric acid concentrations, practically all DMA is used up in particle formation and the slopes with respect to both sulfuric acid and DMA concentrations decrease. On the other hand, the role of ammonia becomes more important at high sulfuric acid concentrations as there is a lot of excess sulfuric acid compared to DMA.

4.7. Practical problems related to analyzing field observations of particle formation events (assumptions E, G and H)

The nucleation rate is not a directly observable quantity, but needs in practice to be calculated from cluster or particle concentration and size distribution measurements. Since clusters are lost by coagulation and deposition during their growth from the critical cluster to detectable particles, formation rate determinations at different cut-off sizes give different results. In order to minimize the effect of losses, the particle formation rate determined at the instrument cut-off size (for instance 3 nm) is often converted to the nucleation rate at the assumed critical cluster size (1 or 1.5 nm) using the formulation of Kerminen & Kulmala (2002).

One critical step when applying this procedure to atmospheric data is determining the cluster growth rate, since the coagulation loss rate depends strongly on cluster size. The growth rate also determines how long the clusters spend in any particular size range, affecting the overall effect of losses. The growth rate has typically been determined from the time shift between the appearance of sulfuric acid and of small particles, which has been interpreted as the time required for freshly nucleated clusters to grow to a detectable size. Using the same aerosol microphysics model as in this study (UHMA), Korhonen et al. (2011) have studied the effect of inaccuracies in determining the cluster growth rate on the estimation of the nucleation rate at the critical size.

In the case of a strong nucleation burst, coagulation losses increase significantly during the event due to the large number of nucleation mode particles, reducing the concentration of the smallest particles. This alters the time profile of the particle concentration compared to cases where losses are dominated by the fairly constant background particle population, and skews the growth time determination resulting systematically in too high values for the growth rate. This, in turn, leads to an underestimation of the nucleation rate, which is most prominent at high nucleation rates, corresponding in general to high sulfuric acid concentrations. Finally, the sulfuric acid dependent bias in the calculated nucleation rate leads to an incorrect estimate of the exponent in the nucleation rate power law and thus an erroneous interpretation of the nucleation mechanism.

We simulated eight events with the UHMA aerosol microphysics model assuming a particle formation rate of the form $J_{1.5,\mathrm{input}} = K[H_2SO_4]^2$. The background particle concentration and the cluster growth rate were varied between the simulations, which corresponds to what happens also in measurement campaigns where events on different days exhibit different conditions. As in Sihto et al. (2006), the particle formation rate J_3 at 3 nm was obtained directly from the time evolution of the particle size distribution and the average growth rate below 3 nm was solved from the time shift between $[H_2SO_4]$ and N_{3-6}. The formation rate $J_{1.5}$ at 1.5 nm was then estimated using the Kerminen & Kulmala (2002) formulation. A detailed description of the methodology was presented by Korhonen et al. (2011).

Figure 9 presents the synthetic measurement campaign of eight events generated with UHMA. Each data point represents a single "measurement" of $[H_2SO_4]$ and the corresponding estimate of $J_{1.5}$. The spread in the $J_{1.5}$ values is due to several factors: each of the eight events represent different conditions with different growth rates and coagulation sinks, the prefactor K varies with time during each event, and finally the analysis method is sensitive to the conditions of the event and does not always reproduce the input formation rate even in more idealized conditions.

Fitting a least-squares line to the estimated nucleation rates gives a slope of 0.92, which is clearly lower than the input exponent 2. Another set of nucleation events with slightly different growth rates or coagulation sinks would have led to a different exponent. Many previous studies of atmospheric new-particle formation have applied the first nucleation theorem to extensive field data by combining nucleation rate data inferred from a large number of events, some (e.g. Metzger et al., 2010) even acknowledging that the conditions for the validity of the nucleation theorem are not met. Our example shows, however, that applying slope analysis to a collection of several independent data sets corresponding to randomly varying atmospheric conditions may lead to a wrong conclusion about the dependence of $J_{1.5}$ on $[H_2SO_4]$. One approach for avoiding the difficulties related to varying conditions was proposed by Laaksonen et al. (2008), who applied multivariate regression analysis to nucleation rates measured in the atmosphere. However, this method requires prior knowledge about all compounds involved in particle formation, and their concentrations must be measured with a sufficient time resolution during the events.

5. Summary and conclusions

Numerous studies have used the first nucleation theorem to assess atmospheric new-particle formation mechanisms. According to the theorem, derived for ideal conditions, the slope of the nucleation rate as a function of the concentration of a nucleating compound is approximately equal to the number of molecules of the compound in the critical cluster. In this work, the sensitivity of the slope to various non-idealities was examined. We used a cluster kinetics model to simulate the formation rate of stable small clusters consisting of sulfuric acid and base molecules. The simulations were performed both in ideal conditions and in realistic conditions where the assumptions related to the nucleation theorem are not valid. Even in otherwise ideal conditions, the ΔG surfaces taken from quantum chemical calculations did not comply to the assumptions made in the derivation of the nucleation theorem. However, in the sulfuric acid–ammonia system where the formation free energy curve has several local maxima along the formation pathway, the nucleation theorem was shown to be very closely valid. On the other hand, any other non-idealities such as external losses of clusters or not reaching a steady-state were seen to destroy the applicability of the theorem. For instance, in the presence of wall losses, slope analysis can indicate the presence of a large critical cluster even when cluster formation is in fact barrierless.

Furthermore, the so-called nucleation rate is in practice calculated from the measured concentrations at larger, experimentally detectable sizes. To assess uncertainties related to the calculation, an aerosol microphysics model was used to simulate the growth of freshly formed particles to detectable sizes. The slope of the calculated nucleation rate as a function of sulfuric acid concentration was found to differ from that of the actual formation rate used as input in the simulation.

The derivation of the nucleation theorem requires that there are no external losses, which is never perfectly true in reality. However, with high enough precursor concentrations and a suitable setup, the effect of losses on the particle formation rate may become negligible. On the other hand, a high precursor concentration may lead to a non-negligible contribution of cluster-cluster collisions, which also breaks the applicability of the nucleation theorem. Even the less restrictive assumptions that the nucleation is in steady-state and that all conditions except for one concentration are kept constant between different measurement points are often not fulfilled. Thus the first nucleation theorem cannot be used to determine the critical cluster size in most realistic situations.

Acknowledgments

We would like to thank Dr. Ismael K. Ortega and Dr. Theo Kurtén for discussions and the Vilho, Yrjö and Kalle Väisälä Foundation, the Academy of Finland (Center of Excellence program Grant #272041, LASTU program project #135054, Research Fellow position #250348), the European Research Council (project ERC-StG 257360-MOCAPAF) and the ACCC doctoral program for funding.

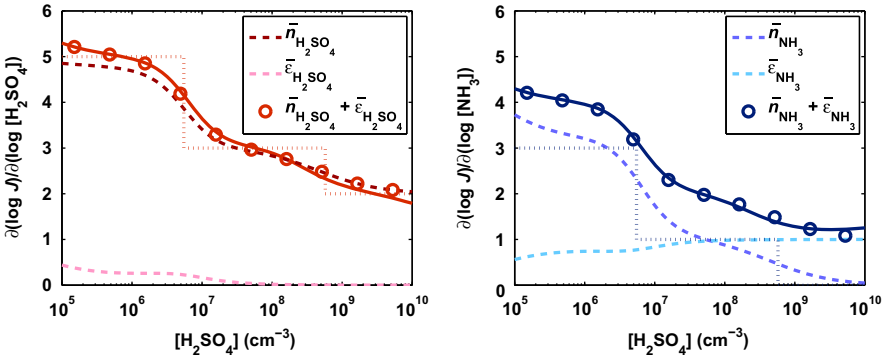

Fig. 10. Logarithmic partial derivatives of the particle formation rate with respect to sulfuric acid and ammonia concentrations (bright red and dark blue solid lines, respectively) at $[NH_3]=10$ ppt compared to the prediction of the nucleation theorem (circles). The dotted lines correspond to the number of H_2SO_4 and NH_3 molecules in the critical cluster, and the dashed lines refer to the terms on the right-hand side of Eq. (9). (For interpretation of the references to color in this figure caption, the reader is referred to the web version of this paper.)

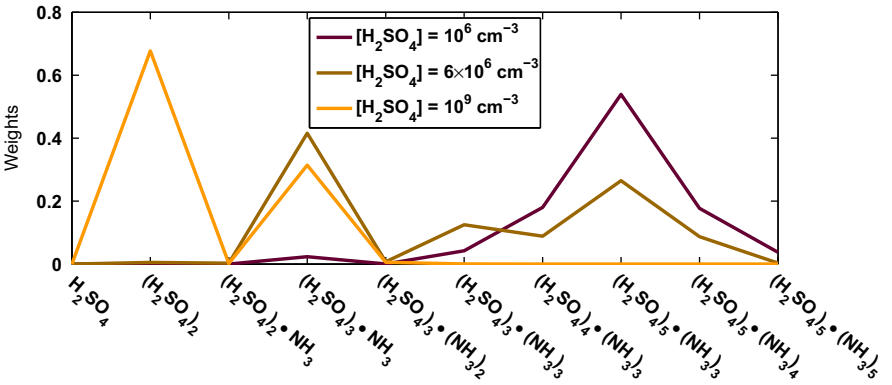

Fig. 11. The distribution $(1/\beta_{m_k,k}C_{m_k}c_{k,0})/\left[\sum_{l=1}^{10} 1/(\beta_{m_l,l}C_{m_l}c_{l,0})\right]$ appearing in Eq. (9) computed at different H_2SO_4 monomer concentrations and $[NH_3]=10$ ppt for the neutral sulfuric acid–ammonia system.

Appendix A

A.1. Validity of the multi-component nucleation theorem Eq. (9)

Figure 10 presents the derivatives from Fig. 1 together with the terms $\bar{n}_i$ and $\bar{\varepsilon}_i$ of Eq. (9). The derivatives with respect to both sulfuric acid and ammonia are very closely equal to $\bar{n}_i+\bar{\varepsilon}_i$, in agreement with the multi-component nucleation theorem. The small discrepancy can be explained by a fraction of the particle formation proceeding along an alternative pathway (see Olenius et al., 2013a for more details). However, while Eq. (9) is approximately valid, it does not give a direct link between the slope of the particle formation rate and the critical cluster size. This can be understood by examining the distribution (shown in Fig. 11) over which the weighted average of cluster compositions is calculated to give $\bar{n}_i$. It is traditionally assumed that the term $1/c_{k,0} \propto \exp\left[\Delta G_k/(k_B T)\right]$ has such a high peak at the location of the energy barrier that this one term dominates the whole sum and $\bar{n}_i \approx n_i^*$, but the example of Fig. 11 shows that several terms, some of which do not even correspond to local maxima of the formation energy curve, may have a non-negligible contribution to the sum. In Fig. 11, the sum in the denominator of Eq. (9) is only computed over the monomer and the nine smallest clusters on the formation pathway, but adding more terms would affect merely the normalization, not the shape, of the distribution.

A.2. Cluster concentrations in the sulfuric acid–DMA system

The cluster concentrations corresponding to Fig. 2 are presented in Fig. 12. Cluster concentrations are overall higher in the hypothetical case where cluster-cluster collisions are forbidden, compared to the case where all collisions are allowed.

A.3. Ion concentrations when the ion production rate is fixed

Figure 13 presents the HSO_4^- and NH_4^+ concentrations corresponding to the constant ion production rate of Fig. 6. At low sulfuric acid concentrations the bisulfate ion concentration increases with increasing sulfuric acid concentration as there are more H_2SO_4 molecules available to get ionized by the charger ions. The NH_4^+ ion concentration, on the other hand, has

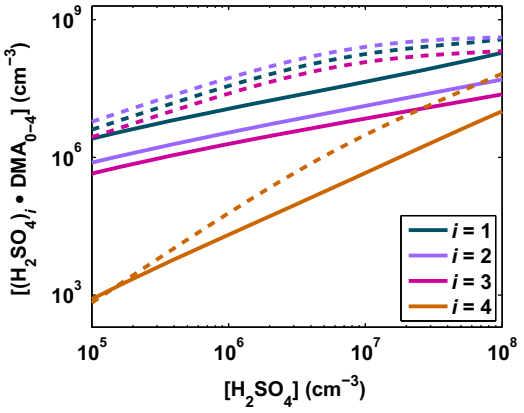

Fig. 12. Concentrations of neutral clusters containing 1, 2, 3 and 4 sulfuric acid molecules and any number of DMA molecules at [DMA]=10 ppt. The solid lines correspond to the case where all collisions are allowed, and the dashed lines correspond to a hypothetical situation where cluster–cluster collisions and fragmentations are forbidden.

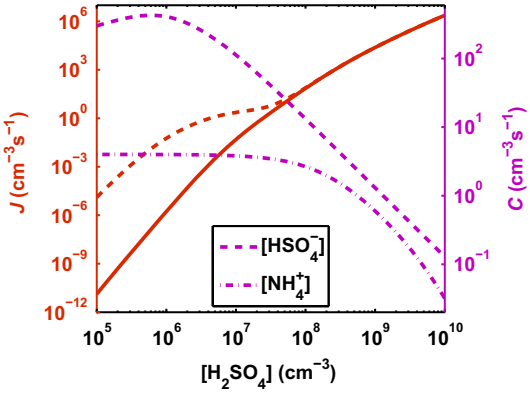

Fig. 13. Particle formation rate at $[NH_3]=10$ ppt with no ions (solid red line) and with an ion production rate IPR=3 ion pairs cm^{-3} s^{-1} (red dashed line), and the bisulfate and ammonium ion concentrations (purple) corresponding to the same ion production rate. (For interpretation of the references to color in this figure caption, the reader is referred to the web version of this paper.)

practically no dependence on the sulfuric acid concentration at low acid concentrations, as the ammonium ions are formed when an ammonia molecule is charged positively, and lost mainly by colliding with a second ammonia molecule and forming an $NH_3 \cdot NH_4^+$ cluster. At higher sulfuric acid concentrations, collisions with H_2SO_4 molecules become an important loss mechanism for both HSO_4^- and NH_4^+ ions, and their concentrations therefore decrease with increasing sulfuric acid concentration.

References

Almeida, J., Schobesberger, S., Kürten, A., Ortega, I.K., Kupiainen-Määttä, O., Praplan, A.P., Adamov, A., Amorim, A., Bianchi, F., Breitenlechner, M., David, A., Dommen, J., Donahue, N.M., Downard, A., Dunne, E., Duplissy, J., Ehrhart, S., Flagan, R.C., Franchin, A., Guida, R., Hakala, J., Hansel, A., Heinritzi, M., Henschel, H., Jokinen, T., Junninen, H., Kajos, M., Kangasluoma, J., Keskinen, H., Kupc, A., Kurtén, T., Kvashin, A.N., Laaksonen, A., Lehtipalo, K., Leiminger, M., Leppä, J., Loukonen, V., Makhmutov, V., Mathot, S., McGrath, M.J., Nieminen, T., Olenius, T., Onnela, A., Petäjä, T., Riccobono, F., Riipinen, I., Rissanen, M., Rondo, L., Ruuskanen, T., Santos, F.D., Sarnela, N., Schallhart, S., Schnitzhofer, R., Seinfeld, J.H., Simon, M., Sipilä, M., Stozhkov, Y., Stratmann, F., Tomé, A., Tröstl, J., Tsagkogeorgas, G., Vaattovaara, P., Viisanen, Y., Virtanen, A., Vrtala, A., Wagner, P.E., Weingartner, E., Wex, H., Williamson, C., Wimmer, D., Ye, P., Yli-Juuti, T., Carslaw, K.S., Kulmala, M., Curtius, J., Baltensperger, U., Worsnop, D.R., Vehkamäki, H., & Kirkby, J. (2013). Molecular understanding of sulphuric acid–amine particle nucleation in the atmosphere. *Nature*, *502*(7471), 359–363, http://dx.doi.org/10.1038/nature12663 ISSN 0028-0836.

Ball, S.M., Hanson, D.R., Eisele, F.L., & McMurry, P.H. (1999). Laboratory studies of particle nucleation: Initial results for H_2SO_4, H_2O, and NH_3 vapors. *Journal of Geophysical Research*, *104*(D19), 23709–23718, http://dx.doi.org/10.1029/1999JD900411.

Barrett, J.C. (2008). A stochastic simulation of nonisothermal nucleation. *Journal of Chemical Physics*, *128*(16), 164519, http://dx.doi.org/10.1063/1.2913051.

Becker, C., & Reiss, H. (1976). Nucleation in a nonuniform vapor. *Journal of Chemical Physics*, *65*, 2066–2070, http://dx.doi.org/10.1063/1.433390.

Benson, D.R., Young, L.-H., Kameel, F.R., & Lee, S.-H. (2008). Laboratory-measured nucleation rates of sulfuric acid and water binary homogeneous nucleation from the SO_2 + OH reaction. *Geophysical Research Letters*, *35*(11), L11801, http://dx.doi.org/10.1029/2008GL033387 ISSN 1944-8007.

Berndt, T., & Richters, S. (2012). Products of the reaction of OH radicals with dimethyl sulphide in the absence of NO_x: experiment and simulation. *Atmospheric Environment*, *47*, 316–322, http://dx.doi.org/10.1016/j.atmosenv.2011.10.060 ISSN 1352-2310.

Brus, D., Hyvärinen, A.P., Zdimal, V., & Lihavainen, H. (2005). Homogeneous nucleation rate measurements of 1-butanol in helium: A comparative study of a thermal diffusion cloud chamber and a laminar flow diffusion chamber. *Journal of Chemical Physics*, *122*, 214506, http://dx.doi.org/10.1063/1.1917746.

Brus, D., Zdimal, V., & Stratmann, F. (2006). Homogeneous nucleation rate measurements of 1-propanol in helium: The effect of carrier gas pressure. *Journal of Chemical Physics*, *124*, 164306, http://dx.doi.org/10.1063/1.2185634.

Brus, D., Hyvärinen, A.-P., Viisanen, Y., Kulmala, M., & Lihavainen, H. (2010). Homogeneous nucleation of sulfuric acid and water mixture: Experimental setup and first results. *Atmospheric Chemistry and Physics*, *10*, 2631–2641, http://dx.doi.org/10.5194/acp-10-2631-2010.

Dal Maso, M., Hyvärinen, A., Komppula, M., Tunved, P., Kerminen, V.-M., Lihavainen, H., Viisanen, Y., Hansson, H.-C., & Kulmala, M. (2008). Annual and interannual variation in boreal forest aerosol particle number and volume concentration and their connection to particle formation. *Tellus B*, *60*(4), 495–508, http://dx.doi.org/10.1111/j.1600-0889.2008.00366.x.

Ehrhart, S., & Curtius, J. (2013). Influence of aerosol lifetime on the interpretation of nucleation experiments with respect to the first nucleation theorem. *Atmospheric Chemistry and Physics*, *13*(22), 11465–11471, http://dx.doi.org/10.5194/acp-13-11465-2013.

Eisele, F., & Tanner, D. (1993). Measurement of the gas phase concentration of H_2SO_4 and methane sulfonic acid and estimates of H_2SO_4 production and loss in the atmosphere. *Journal of Geophysical Research*, *98*(D5), 9001–9010, http://dx.doi.org/10.1029/93JD00031.

Ford, I.J. (1997). Nucleation theorems, the statistical mechanics of molecular clusters, and a revision of classical nucleation theory. *Physical Review E*, *56*(5), 5615–5629, http://dx.doi.org/10.1103/PhysRevE.56.5615.

Fransen, M.A.L.J., Sachteleben, E., Hrubý, J., & Smeulders, D.M.J. (2013). Homogeneous nucleation of water in synthetic air, *The* 19*th International Conference* on *Nucleation and Atmospheric Aerosol*, *AIP Conference Proceedings*, Vol. 1527. AIP Publishing, Melville, New York, pp. 124–127. ISBN 978-0-7354-1152-4, http://dx.doi.org/10.1063/1.4803219.

Ge, X., Wexler, A.S., & Clegg, S.L. (2011). Atmospheric amines—Part I. A review. *Atmospheric Environment*, *45*(3), 524–546, http://dx.doi.org/10.1016/j.atmosenv.2010.10.012.

Hanson, D.R., & Eisele, F. (2000). Diffusion of H_2SO_4 in humidified nitrogen: Hydrated H_2SO_4. *Journal of Physical Chemistry A*, *104*(8), 1715–1719, http://dx.doi.org/10.1021/jp993622j.

Hrubý, J., Viisanen, Y., & Strey, R. (1996). Homogeneous nucleation rates for n-pentanol in argon: Determination of the critical cluster size. *Journal of Chemical Physics*, *104*(13), 5181–5187, http://dx.doi.org/10.1063/1.471145.

Kashchiev, D. (1982). On the relation between nucleation work, nucleus size, and nucleation rate. *Journal of Chemical Physics*, *76*(10), 5098–5102, http://dx.doi.org/10.1063/1.442808.

Kerminen, V.-M., & Kulmala, M. (2002). Analytical formulae connecting the "real" and the "apparent" nucleation rate and the nuclei number concentration for atmospheric nucleation events. *Journal of Aerosol Science*, *33*(4), 609–622, http://dx.doi.org/10.1016/S0021-8502(01)00194-X.

Kim, Y.J., Wyslouzil, B.E., Wilemski, G., Wölk, J., & Strey, R. (2004). Isothermal nucleation rates in supersonic nozzles and the properties of small water clusters. *Journal of Physical Chemistry A*, *108*, 4365–4377, http://dx.doi.org/10.1021/jp037030j.

Kirkby, J., Curtius, J., Almeida, J., Dunne, E., Duplissy, J., Ehrhart, S., Franchin, A., Gagné, S., Ickes, L., Kürten, A., Kupc, A., Metzger, A., Riccobono, F., Rondo, L., Schobesberger, S., Tsagkogeorgas, G., Wimmer, D., Amorim, A., Bianchi, F., Breitenlechner, M., David, A., Dommen, J., Downard, A., Ehn, M., Flagan, R.C., Haider, S., Hansel, A., Hauser, D., Jud, W., Junninen, H., Kreissl, F., Kvashin, A., Laaksonen, A., Lehtipalo, K., Lima, J., Lovejoy, E.R., Makhmutov, V., Mathot, S., Mikkilä, J., Minginette, P., Mogo, S., Nieminen, T., Onnela, A., Pereira, P., Petaja, T., Schnitzhofer, R., Seinfeld, J.H., Sipilä, M., Stozhkov, Y., Stratmann, F., Tomé, A., Vanhanen, J., Viisanen, Y., Vrtala, A., Wagner, P.E., Walther, H., Weingartner, E., Wex, H., Winkler, P.M., Carslaw, K.S., Worsnop, D.R., Baltensperger, U., & Kulmala, M. (2011). Role of sulphuric acid, ammonia and galactic cosmic rays in atmospheric aerosol nucleation. *Nature*, *476*, 429, http://dx.doi.org/10.1038/nature10343 ISSN 0028-0836.

Korhonen, H., Lehtinen, K.E.J., & Kulmala, M. (2004). Multicomponent aerosol dynamics model UHMA: Model development and validation. *Atmospheric Chemistry and Physics*, *4*, 757–771, http://dx.doi.org/10.5194/acp-4-757-2004.

Korhonen, H., Sihto, S.-L., Kerminen, V.-M., & Lehtinen, K.E.J. (2011). Evaluation of the accuracy of analysis tools for atmospheric new particle formation. *Atmospheric Chemistry and Physics*, *11*(7), 3051–3066, http://dx.doi.org/10.5194/acp-11-3051-2011.

Korhonen, H., Kerminen, V.-M., Kokkola, H., & Lehtinen, K.E.J. (2014). Estimating atmospheric nucleation rates from size distribution measurements: Analytical equations for the case of size dependent growth rates. *Journal of Aerosol Science*, *69*, 13–20, http://dx.doi.org/10.1016/j.jaerosci.2013.11.006 ISSN 0021-8502.

Kuang, C., McMurry, P.H., McCormick, A.V., & Eisele, F.L. (2008). Dependence of nucleation rates on sulfuric acid vapor concentration in diverse atmospheric locations. *Journal of Geophysical Research*, *113*, D10209, http://dx.doi.org/10.1029/2007JD009253.

Kuang, C., Chen, M., Zhao, J., Smith, J., McMurry, P.H., & Wang, J. (2012). Size and time-resolved growth rate measurements of 1 to 5 nm freshly formed atmospheric nuclei. *Atmospheric Chemistry and Physics*, *12*, 3573–3589, http://dx.doi.org/10.5194/acp-12-3573-2012.

Kulmala, M., Vehkamäki, H., Petäjä, T., Dal Maso, M., Lauri, A., Kerminen, V.-M., Birmili, W., & McMurry, P.H. (2004). Formation and growth rates of ultrafine atmospheric particles: A review of observations. *Journal of Aerosol Science*, *35*, 143–176, http://dx.doi.org/10.1016/j.jaerosci.2003.10.003.

Kupiainen, O., Olenius, T., & Vehkamäki, H. (2013). Experimental setup affects the particle formation rate and its slope d(log *J*)/d(log *C*), *The* 19*th International Conference on Nucleation and Atmospheric Aerosols, AIP Conference Proceedings*, Vol. 1527. AIP Publishing, Melville, New York, pp. 246–249. ISBN 978-0-7354-1152-4, http://dx.doi.org/10.1063/1.4803250.

Kupiainen-Määttä, O., Olenius, T., Kurtén, T., & Vehkamäki, H. (2013). CIMS sulfuric acid detection efficiency enhanced by amines due to higher dipole moments—A computational study. *Journal of Physical Chemistry A*, *117*(51), 14109–14119, http://dx.doi.org/10.1021/jp4049764.

Kurtén, T., Kuang, C., Gómez, P., McMurry, P.H., Vehkamäki, H., Ortega, I.K., Noppel, M., & Kulmala, M. (2010). The role of cluster energy nonaccommodation in atmospheric sulfuric acid nucleation. *Journal of Chemical Physics*, *132*, 024304, http://dx.doi.org/10.1063/1.3291213.

Laaksonen, A., Kulmala, M., Berndt, T., Stratmann, F., Mikkonen, S., Ruuskanen, A., Lehtinen, K.E.J., Dal Maso, M., Aalto, P., Petäjä, T., Riipinen, I., Sihto, S.-L., Janson, R., Arnold, F., Hanke, M., Ucker, J., Umann, B., Sellegri, K., O'Dowd, C.D., & Viisanen, Y. (2008). SO_2 oxidation products other than H_2SO_4 as a trigger of new particle formation. Part 2: Comparison of ambient and laboratory measurements, and atmospheric implications. *Atmospheric Chemistry and Physics*, *8*(23), 7255–7264, http://dx.doi.org/10.5194/acp-8-7255-2008.

Lehtinen, K.E.J., Dal Maso, M., Kulmala, M., & Kerminen, V.-M. (2007). Estimating nucleation rates from apparent particle formation rates and vice versa: Revised formulation of the Kerminen–Kulmala equation. *Journal of Aerosol Science*, *38*(9), 988–994, http://dx.doi.org/10.1016/j.jaerosci.2007.06.009 ISSN 0021-8502.

Leverentz, H.R., Siepmann, J.I., Truhlar, D.G., Loukonen, V., & Vehkamäki, H. (2013). Energetics of atmospherically implicated clusters made of sulfuric acid, ammonia, and dimethyl amine. *Journal of Physical Chemistry A*, *117*(18), 3819–3825, http://dx.doi.org/10.1021/jp402346u.

Li, J.-S., Maksimov, I.L., & Wilemski, G. (2000). Genuine saddle point and nucleation potential for binary systems. *Physical Review E*, *61*(5), R4710–R4713, http://dx.doi.org/10.1103/PhysRevE.61.R4710.

Loukonen, V., Bork, N., & Vehkamäki, H. (2014a). From collisions to clusters: First steps of sulfuric acid nanocluster formation dynamics,*Molecular Physics: An International Journal at the Interface BetweenChemistry and Physics,* http://dx.doi.org/10.1080/00268976.2013.877167.

Loukonen, V., Kuo, I.-F.W., McGrath, M.J., & Vehkamäki, H. (2014b). On the stability and dynamics of (sulfuric acid) (ammonia) and (sulfuric acid) (dimethylamine) clusters: A first-principles molecular dynamics investigation. *Chemical Physics*, *428*, 164–174. http://dx.doi.org/10.1016/j.chemphys.2013.11.014.

Malila, J., Lehtinen, K., Napari, I., McGraw, R., & Laaksonen, A. (2011). Coagulation scavenging of precritical clusters and the first nucleation theorem, *European Aerosol Conference* 2011, abstract number 4P59.

Malila, J., McGraw, R., Laaksonen, A., & Lehtinen, K.E.J. (2013). Repairing the first nucleation theorem: Precritical cluster losses, *The* 19*th International Conference on Nucleation and Atmospheric Aerosols*, *AIP Conference Proceedings*, Vol. 1527. AIP Publishing, Melville, New York, pp. 31–34. ISBN 978-0-7354-1152-4, http://dx.doi.org/10.1063/1.4803197.

Malila, J., McGraw, R., Laaksonen, A., & Lehtinen, K.E.J. (2014). Kinetics of scavenging of small, nucleating clusters: First nucleation theorem and sum rules, in revision.

Manka, A.A., Brus, D., Hyvärinen, A.P., Lihavainen, H., Wölk, J., & Strey, R. (2010). Homogeneous water nucleation in a laminar flow diffusion chamber. *Journal of Chemical Physics*, *132*(24), 244505, http://dx.doi.org/10.1063/1.3427537.

McGrath, M.J., Olenius, T., Ortega, I.K., Loukonen, V., Paasonen, P., Kurtén, T., Kulmala, M., & Vehkamäki, H. (2012). Atmospheric cluster dynamics code: A flexible method for solution of the birth–death equations. *Atmospheric Chemistry and Physics*, *12*, 2345–2355, http://dx.doi.org/10.5194/acp-12-2345-2012.

McGraw, R., & Wu, D.T. (2003). Kinetic extensions of the nucleation theorem. *Journal of Chemical Physics*, *118*(20), 9337–9347, http://dx.doi.org/10.1063/1.1565098.

McGraw, R., & Zhang, R. (2008). Multivariate analysis of homogeneous nucleation rate measurements. Nucleation in the p-toluic acid/sulfuric acid/water system. *Journal of Chemical Physics*, *128*(6), 064508, http://dx.doi.org/10.1063/1.2830030.

Metzger, A., Verheggen, B., Dommen, J., Duplissy, J., Prevot, A.S.H., Weingartner, E., Riipinen, I., Kulmala, M., Spracklen, D.V., Carslaw, K.S., & Baltensperger, U. (2010). Evidence for the role of organics in aerosol particle formation under atmospheric conditions. *Proceedings of the National Academy of Sciences of the United States of America*, *107*(15), 6646–6651, http://dx.doi.org/10.1073/pnas.0911330107.

Nadykto, A., Yu, F., Jakovleva, M., Herb, J., & Xu, Y. (2011). Amines in the earth's atmosphere: A density functional theory study of the thermochemistry of pre-nucleation clusters. *Entropy*, *13*, 554–569, http://dx.doi.org/10.3390/e13020554.

Nielsen, A.E. (1964). *Kinetics of Precipitation. International Series of Monographs in Analytical Chemistry*, Vol. 18. Pergamon Press: Oxford.

Olenius, T., Kupiainen-Määttä, O., Ortega, I.K., Kurtén, T., & Vehkamäki, H. (2013a). Free energy barrier in the growth of sulfuric acid–ammonia and sulfuric acid–dimethylamine clusters. *Journal of Chemical Physics*, *139*(8), 084312, http://dx.doi.org/10.1063/1.4819024.

Olenius, T., Schobesberger, S., Kupiainen-Määttä, O., Franchin, A., Junninen, H., Ortega, I.K., Kurtén, T., Loukonen, V., Worsnop, D.R., Kulmala, M., & Vehkamäki, H. (2013b). Comparing simulated and experimental molecular cluster distributions. *Faraday Discussions*, *165*, 75–89, http://dx.doi.org/10.1039/c3fd00031a.

Ortega, I.K., Kupiainen, O., Kurtén, T., Olenius, T., Wilkman, O., McGrath, M.J., Loukonen, V., & Vehkamäki, H. (2012). From quantum chemical formation free energies to evaporation rates. *Atmospheric Chemistry and Physics*, *12*, 225–235, http://dx.doi.org/10.5194/acp-12-225-2012.

Riipinen, I., Sihto, S.-L., Kulmala, M., Arnold, F., Dal Maso, M., Birmili, W., Saarnio, K., Teinilä, K., Kerminen, V.-M., Laaksonen, A., & Lehtinen, K.E.J. (2007). Connections between atmospheric sulphuric acid and new particle formation during QUEST III–IV campaigns in Heidelberg and Hyytiälä. *Atmospheric Chemistry and Physics*, *7*, 1899–1914, http://dx.doi.org/10.5194/acp-7-1899-2007.

Shampine, L., & Reichelt, M. (1997). The MATLAB ODE suite. *SIAM Journal on Scientific Computing*, *18*(1), 1–22, http://dx.doi.org/10.1137/S1064827594276424.

Sihto, S.-L., Kulmala, M., Kerminen, V.-M., Dal Maso, M., Petäjä, T., Riipinen, I., Korhonen, H., Arnold, F., Janson, R., Boy, M., Laaksonen, A., & Lehtinen, K.E.J. (2006). Atmospheric sulphuric acid and aerosol formation: Implications from atmospheric measurements for nucleation and early growth mechanisms. *Atmospheric Chemistry and Physics*, *6*, 4079–4091, http://dx.doi.org/10.5194/acp-6-4079-2006.

Sipilä, M., Berndt, T., Petäjä, T., Brus, D., Vanhanen, J., Stratmann, F., Patokoski, J., Mauldin, R.L., Hyvärinen, A.-P., Lihavainen, H., & Kulmala, M. (2010). The role of sulfuric acid in atmospheric nucleation. *Science*, *327*, 1243–1246, http://dx.doi.org/10.1126/science.1180315.

Strey, R., & Viisanen, Y. (1993). Measurement of the molecular content of binary nuclei—Use of the nucleation rate surface for ethanol–hexanol. *Journal of Chemical Physics*, *99*(6), 4693–4704, http://dx.doi.org/10.1063/1.466067.

Su, T., & Chesnavich, W.J. (1982). Parametrization of the ion–polar molecule collision rate constant by trajectory calculations. *Journal of Chemical Physics*, *76*(10), 5183–5185, http://dx.doi.org/10.1063/1.442828.

Vehkamäki, H., & Ford, I.J. (2001). Excess energies of n- and i-octane molecular clusters. *Journal of Chemical Physics*, *114*(13), 5509–5513, http://dx.doi.org/10.1063/1.1351874.

Vehkamäki, H., McGrath, M.J., Kurtén, T., Julin, J., Lehtinen, K.E.J., & Kulmala, M. (2012). Rethinking the application of the first nucleation theorem to particle formation. *Journal of Chemical Physics*, *136*, 094107, http://dx.doi.org/10.1063/1.3689227.

Viisanen, Y., & Strey, R. (1994). Homogeneous nucleation rates for n-butanol. *Journal of Chemical Physics*, *101*(9), 7835–7843, http://dx.doi.org/10.1063/1.468208.

Weber, R.J., Marti, J.J., McMurry, P.H., Eisele, F.L., Tanner, D.J., & Jefferson, A. (1996). Measured atmospheric new particle formation rates: Implications for nucleation mechanisms. *Chemical Engineering Communications.*, *151*, 53–64, http://dx.doi.org/10.1080/00986449608936541.

Wyslouzil, B.E., & Wilemski, G. (1995). Binary nucleation kinetics. II. Numerical solution of the birth-death equations. *Journal of Chemical Physics*, *103*(3), 1137–1151, http://dx.doi.org/10.1063/1.469824.

Wyslouzil, B.E, & Wilemski, G. (1996). Binary nucleation kinetics. III. Transient behavior and time lags. *Journal of Chemical Physics*, *105*(3), 1090–1100, http://dx.doi.org/10.1063/1.471953.

Young, L.H., Benson, D.R., Kameel, F.R., Pierce, J.R., Junninen, H., Kulmala, M., & Lee, S.-H. (2008). Laboratory studies of H_2SO_4/H_2O binary homogeneous nucleation from the SO_2 + OH reaction: Evaluation of the experimental setup and preliminary results. *Atmospheric Chemistry and Physics*, *8*, 4997–5016, http://dx.doi.org/10.5194/acp-8-4997-2008.

Zhang, R. (2010). Getting to the critical nucleus of aerosol formation. *Science*, *328*, 1366–1367, http://dx.doi.org/10.1126/science.1189732.

Zhang, R., Khalizov, A., Wang, L., Hu, M., & Xu, W. (2012). Nucleation and growth of nanoparticles in the atmosphere. *Chemical Reviews*, *112*, 1957–2011, http://dx.doi.org/10.1021/cr2001756.

Zollner, J.H., Glasoe, W.A., Panta, B., Carlson, K.K., McMurry, P.H., & Hanson, D.R. (2012). Sulfuric acid nucleation: Power dependencies, variation with relative humidity, and effect of bases. *Atmospheric Chemistry and Physics*, *12*, 4399–4411, http://dx.doi.org/10.5194/acp-12-4399-2012.